Development of new Methods for Analysis of LPT Data with Application to High-subsonic Jet Measurements

Philipp Godbersen[1,*], Peter Manovski[2], Matteo Novara[1], Daniel Schanz[1], Reinhard Geisler[1], Andreas Schröder[1,3]

1: German Aerospace Center (DLR), Institute of Aerodynamics and Flow Technology, Göttingen, Germany
2: Defence Science and Technology Group, Melbourne, Australia
3: Brandenburgisch Technische Universität (BTU) Cottbus-Senftenberg, Germany
*Corresponding author: Philipp.Godbersen@dlr.de

Keywords: Turbulent Jet, Shake-The-Box, Data Analysis, Lagrangian Particle Tracking.

ABSTRACT

Lagrangian particle tracking enables the accurate measurement of the position, velocity and acceleration of particles moving within fluid flows. Beyond the particle positions in each time step, an actual track of the individual particle is available over time. This can be exploited for new analysis methods that use this continuous nature of the tracks to improve binned statistics of the flow. Instead of considering just particle positions at each sampling time instance the movement of the tracked particle between those time steps can provide additional information. In the case of binning based averaging methods this results in better convergence of the statistics for a given amount of data. We apply such methods to a multi-pulse Shake-The-Box (STB) measurement of a Mach 0.84 jet in air and generate high resolution two-point correlation maps of the flow. Coherent structures in the shear layer are further investigated using event orientated conditional averaging based on quadrant analysis. As a novel approach for using the Lagrangian nature of the measurement data, we additionally show a control volume balance based calculation approach, which together with bin based statistics could provide a pathway towards investigating balance equations of flow quantities.

1. Introduction

By using Lagrangian particle tracking the position, velocity and acceleration of particles moving within fluid flows can be measured accurately. Improving on initial developments for 3D particle tracking velocimetry (PTV) (Maas et al., 1993) the current Shake-The-Box (STB, Schanz et al. (2016)) technique provides Lagrangian particle tracking at high seeding densities providing a wealth of information about the flow. Development of the multi-pulse STB approach (Novara et al., 2016) has opened up this technique for faster flows as well. The individually tracked particles, corresponding to individually tracked fluid parcels, provide ample opportunity for advanced data analysis approaches.

We present results from a large multi-pulse STB measurement campaign of a high sub-sonic jet with multiple nozzle types (Figure 1). Some prior work on a subset of this experiment has already

been published (Godbersen et al., 2019; Manovski et al., 2021) however these have focused on the standard round nozzle case, whereas in this work we will provide a closer look on the effects of a chevron nozzle, as well as a more complete evaluation of the entire available data using advanced analysis approaches. A recent work by Sellappan et al. (2020) also studies high velocity jets using multi-pulse STB, however with a different focus, they investigate slower jets using only round nozzles.

LPT already provides advantages over Eulerian correlation-based techniques. Instead of a fixed regular grid of correlation windows, whose size imposes a low pass filtering effect on resolvable structures, particle positions are distributed in a stochastic manner and provide local point measurements. This can be exploited in ensemble averaging using spatial binning to realize very fine resolutions, since the bin size is not directly linked to the measurement technique and is primarily limited by the amount of available data. A more advanced approach that also considers the additional temporal information available from the actual Lagrangian tracks leads to the concept of functional binning (Godbersen & Schröder, 2020). Considering the bins as well as tracks as continuous functions allows for large amount of flexibility in terms of bin shape and placement, the involvement of uncertainty quantification, and improved convergence. By expressing the statistics within this new framework, we are able to extract higher quality results. In our prior work introducing this approach we have mostly relied on synthetic experiment data so this jet measurement provides an opportunity to showcase the method on a large real-world measurement. Additionally, we will use a conditional averaging approach, based on quadrant analysis as well as introduce a new method for using LPT data with control volumes to calculate balance equations for kinetic energy, momentum or similar quantities.

2. Experiment Setup

The experiments were carried out in the Aeroacoustics Test Facility (SAG) at the German Aerospace Center (DLR) in Göttingen. Two different nozzle geometries, each with an inner diameter D_j of $15\,\mathrm{mm}$ and a lip thickness of $3\,\mathrm{mm}$ were investigated. A round nozzle as well as a chevron nozzle with six notches, both having an inner geometry described by a seventh order polynomial. A detailed description of both nozzles used is given by Miguel & Henning (2013). To accurately set the flow conditions of the jet (that is, nozzle pressure ratio and nozzle temperature) a differential pressure manometer (*Greisinger GDH-14A*) as well as a thermocouple (*8RS Pro Thermoelement Type K*) were used. Two different Mach numbers were investigated, M = 0.506 and M = 0.845. The nozzle is movable in the axial direction enabling different measurement positions along the jet axis. During the course of the experiment, three different positions were investigated, one being close to the nozzle, the other covering the end of the potential core and the last further downstream. The three positions are partially overlapping, allowing for full coverage from the nozzle up to $11D_j$ downstream. The volumetric flow-field of the jet was captured using the multi pulse variant of the STB technique as described by Novara et al. (2016). A combination of two dual frame acquisition

Figure 1. Pictures of the two nozzle types used in the experiment. Same as in (Miguel & Henning, 2013)

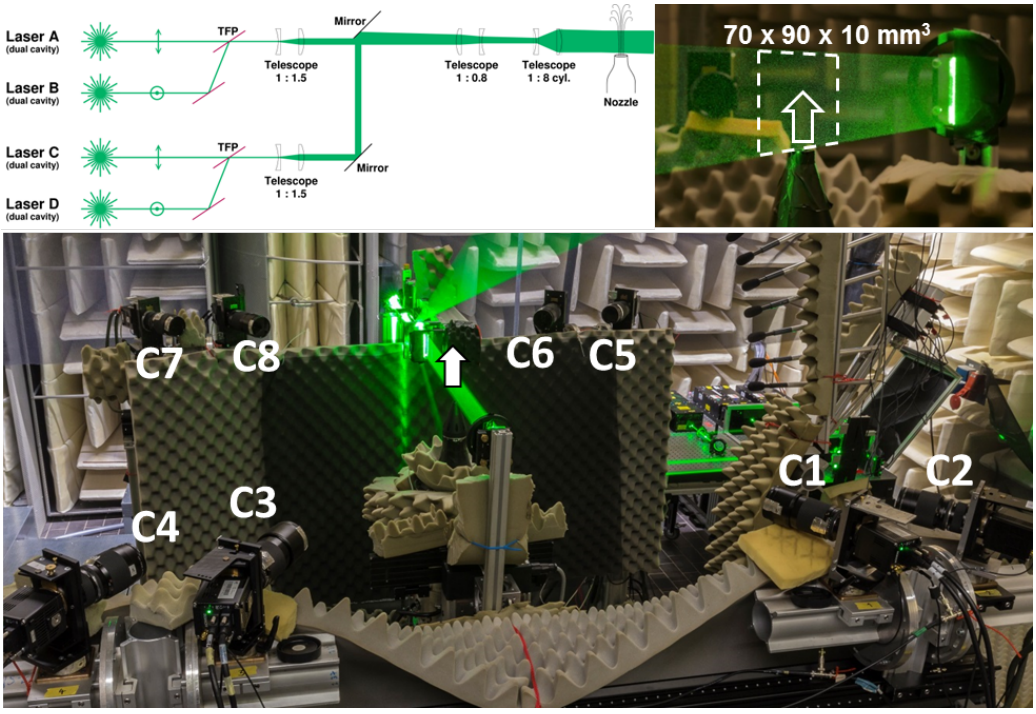

Figure 2. Pictures of the experiment setup showing the camera system arrangement and measurement volume. A diagram of the Illumination setup is provided in the top left corner Manovski et al. (2021)

systems separated by polarization filters is used to capture images of tracer particles illuminated in a $90 \times 70 \times 10\,\mathrm{mm}^3$ volume using a $10\,\mathrm{Hz}$ frame rate. Illumination is provided by two dual-cavity BigSky Evergreen Nd:YAG lasers and two dual-cavity BigSky CFR400 Nd:YAG lasers emitting horizontal and vertical polarized light respectively. In order to increase the available laser energy each pulse of the Evergreen lasers is combined with one pulse of the CFR400 lasers resulting in a total energy per pulse of approximately $400\,\mathrm{mJ}$ with the whole system being capable of four pulses in quick succession. A schematic of the laser setup is given in Figure 2. The laser sheet was also back reflected in order further increase the available illumination and to even out image intensity variations on the camera images caused by the Mie scattering lobes. The timing scheme of the lasers is set up as a four-pulse sequence where the time separation between pulses 1 and 2, and that between pulses 3 and 4 is kept the same and a longer time interval separates pulses 2 and 3. A more detailed description of the measurement setup can be found in (Manovski et al., 2021).

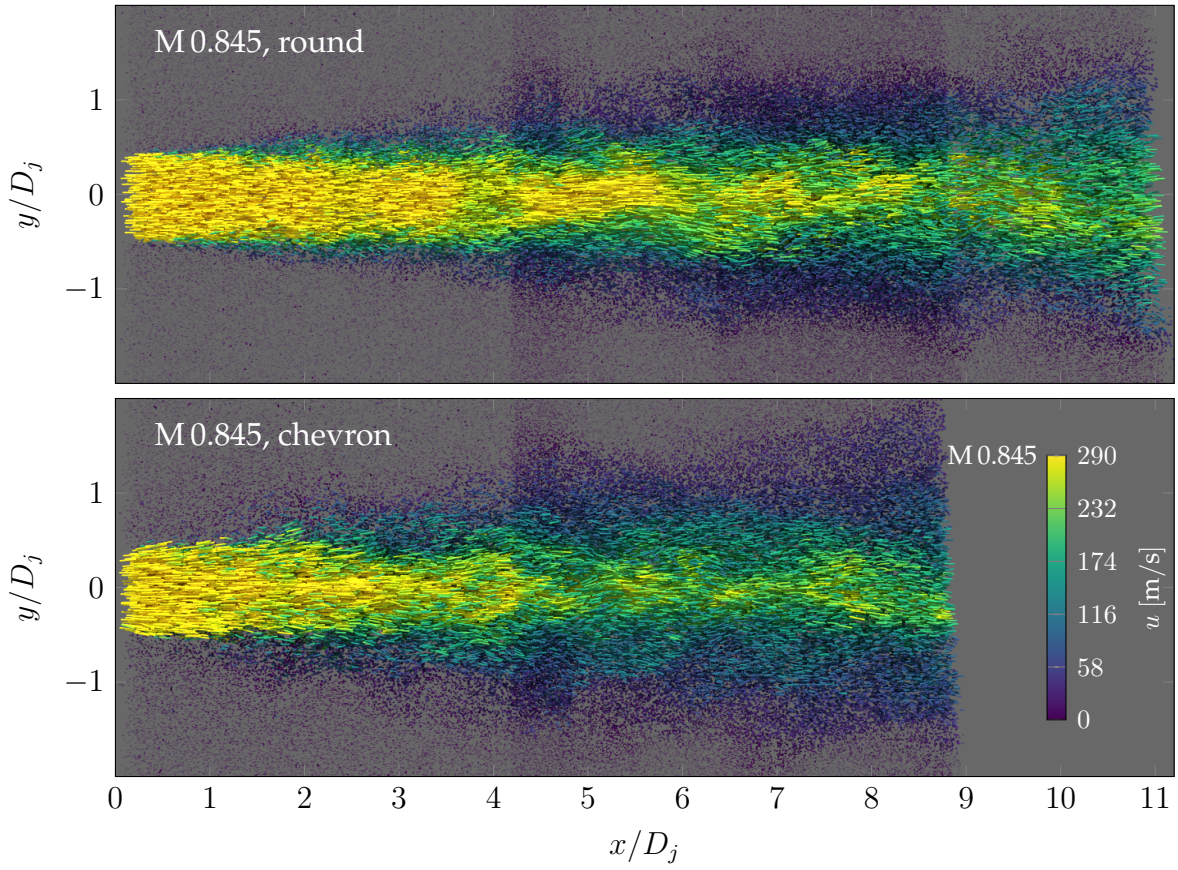

Figure 3. Montage of instantaneous tracks colored by axial velocity. Adapted from (Godbersen et al., 2019)

3. Evaluation

Figure 3 shows an overview of the instantaneous particle tracks recovered for the different jet configurations. For these visualizations, the snapshots at the different measurement positions have been combined together in order to give an overall impression of the extent of the measurement range and the flow-field. These snapshots do not correspond to the same instant in time. The figures have been truncated in the radial direction for better display, the actual measurement space extends more than three nozzle diameters to each radial side. Both jet configurations with the round nozzle are captured up to eleven nozzle diameters in the axial direction while the chevron variants reach up to nine. Instead of visualizing individual snapshots we now consider flow statistics created by bin averaging. An overview over the flow fields for the two nozzle configurations can be achieved by examining the flow statistics from a 3D spatial binning at resolution of 0.4mm. Figure 4 shows the mean axial velocity for the two nozzle types in a cut through the central plane. Differences in the flow profiles are readily apparent. The chevron nozzle exhibits a wider shear layer downstream and a shorter potential core. The jet diameter appears smaller than in the round case but this can be explained by the positioning of the central cut plane placed at z/d=0 visualized here in relation to the notches of the chevron nozzle. The pattern created by the six-notched chevron nozzle can be seen more clearly in the axis normal cut shown in figure 5. There the star

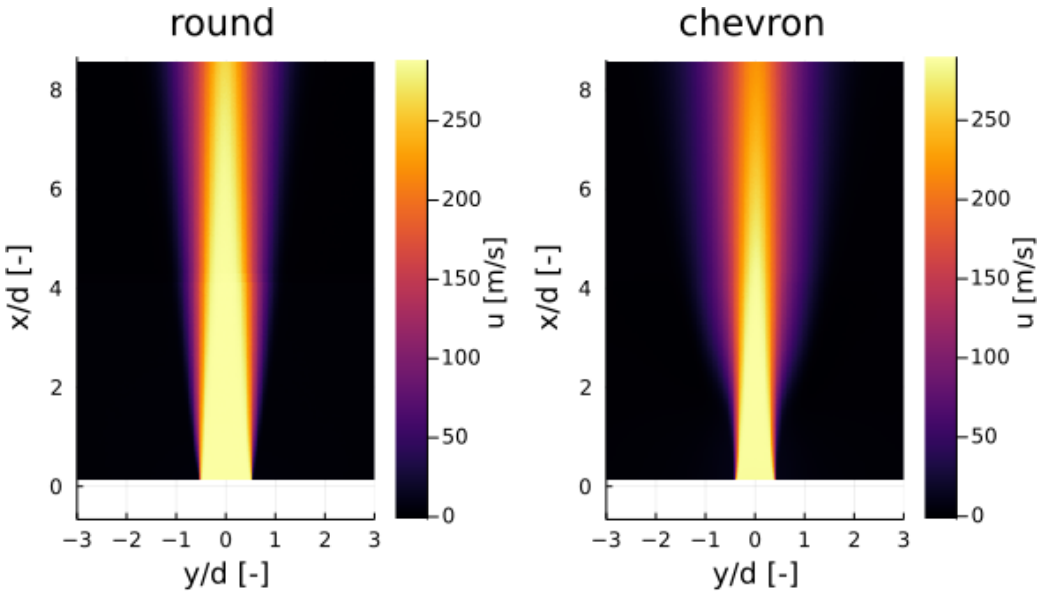

Figure 4. Mean axial velocity in the central cut plane for both nozzle types

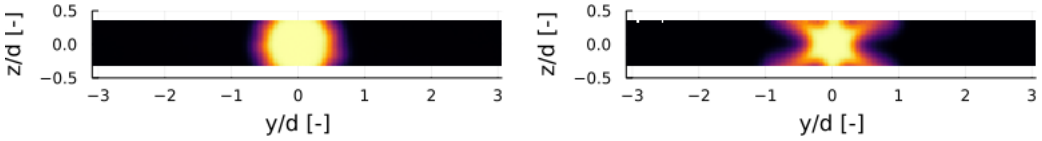

Figure 5. Mean axial velocity in cut plane at x/d=2 for both nozzle types. Same as colorbar as in figure 4.

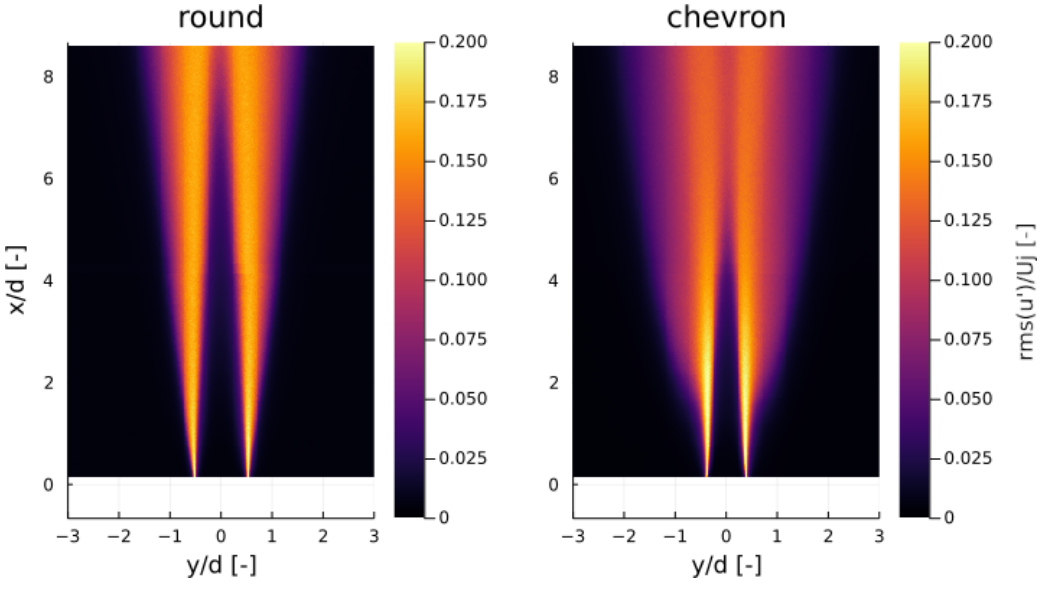

Figure 6. Axial velocity fluctuation rms(u')/Uj in the central cut plane at z/d=0 for both nozzle types

shaped pattern created by the nozzle is apparent. The central cut plane at z/d=0 is positioned directly across the inner notches. As expected from the mean velocity value profile in figure 4, the visualization of the axial velocity fluctuation in figure 6 highlights the differences between the two nozzle types showing the different shear layer profiles. An initially more intense fluctuation for the chevron nozzle subsides further downstream where it is lower compared to the round nozzle. The shorter potential core is even more visible in figure 4.

A better view on the shear layer close to the nozzle can be gained by 1D profiles of the flow statistics. An advantage of LPT data is the easy exploitation of known flow symmetries simply by introducing a coordinate transformation on the particle data. For the round nozzle cylindrical bins capture the experiment well (Manovski et al., 2021). Lagrangian approaches are very well suited for ensemble averaging as particle positions are distributed in a stochastic manner between individual snapshots. Instead of the binning resolution being predefined by correlation-windows in a Eulerian grid like for PIV, the maximum resolution for an ensemble average from scattered particles is theoretically limited only by the amount of snapshots available and the particle position measurement error. In addition to this, we now employ the Functional Binning approach (Godbersen & Schröder, 2020) to achieve even greater resolutions with the same amount of data. The method combines the use of uncertainty quantification, flexible bin design and optimal use of available track data into one complete framework. In figure 7 the advantage of functional binning over a midpoint (classical) binning approach can be seen. For a given number of snapshots and the same bin size the functional approach results in smoother better resolved profiles. The better convergence can be seen by intentionally using a low number of snaphots for evaluation in figure 7 a). But also for a large number of snaphots used benefits remain as can be seen in figure 7 b), where a smoother peak region is achieved as the classical case is not fully converged in that region for this amount of data. Using this approach high resolution velocity mean and fluctuation profiles can be extracted. Figure 8 shows such profiles using now approximately 50,000 snaphots for two positions along the axial direction close to the nozzle.

Beyond the one-point statistics shown, the functional view also allows for the calculation of two-point statistics. Figure 9 shows two-point correlations for a reference point in the shear layer of the jet highlighting coherent structures. The reference point is located approximately 4 nozzle diameters downstream of the nozzle on the lip-line. The auto-correlation for the axial velocity R_{uu} exhibits an elongated correlation region aligned at a slight angle to the axial direction. This is consistent with expectations for a shear layer with the high momentum region on the inside and the high momentum region on the outside in the radial direction. The radial velocity auto-correlation R_{vv} is comprised of a smaller region, elongated more in the radial direction and with negative correlation regions above and below it, a similar arrangement can be seen for the transverse auto-correlation R_{ww} albeit angled. Together these correlations describe the structures in the shear layer where high momentum fluid from the inside is brought towards the outside and paired with this and exchange of low momentum fluid from the outside towards the inside direction. All these correlation maps are generated by exploiting the functional nature of the tracks to improve convergence. For a given bin resolution the functional view allows for smoother statistics as can be

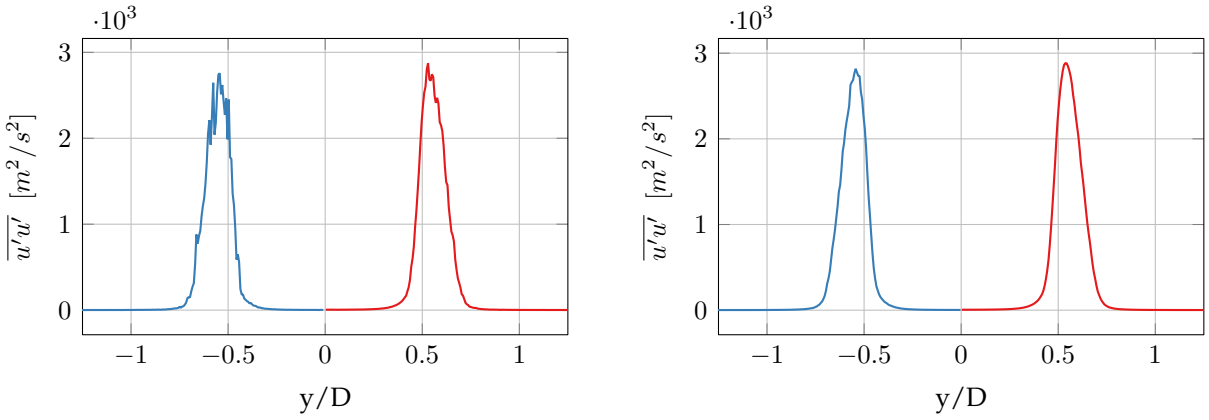

(a) Using only 1000 snapshots

(b) Using 30 000 snapshots

Figure 7. Comparison of the functional to midpoint binning approach for the jet with round nozzle. Axial Reynolds stress profile located ca. 1.5 nozzle diameters downstream. Using 3px bin size in axial and radial direction. —Midpoint; —Functional. (Godbersen & Schröder, 2021)

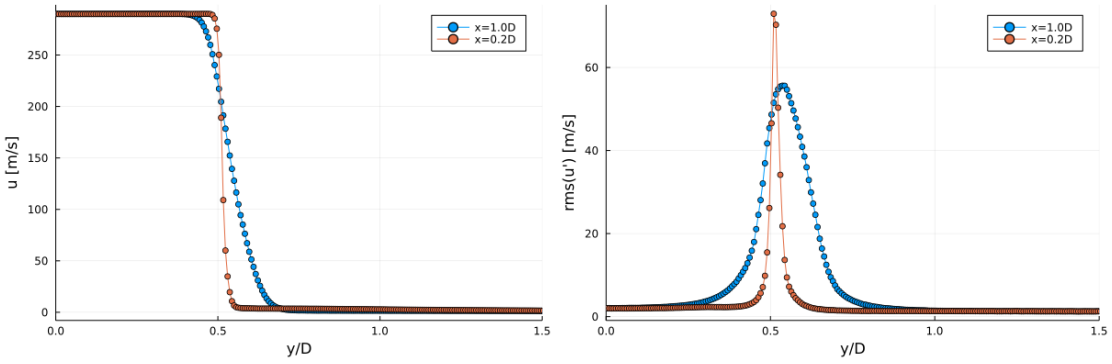

Figure 8. Mean velocity (left) and velocity fluctuation (right) profiles calculated using functional binning at two axial positions with a bin size of 0.1mm using approx. 50,000 snaphots

seen in figure 10, where a comparison is made with the classic approach that utilizes only information at particle positions in each timestep.

One additional advantage of working with LPT data is the availability of data assimilation approaches such as the FlowFit technique (Gesemann et al., 2016) which allows interpolation of the Lagrangian data onto a Eulerian grid utilizing physics-based constraints. This means both Eulerian and Lagrangian interpretations for a given measurement are available and analyses that benefit from a Eulerian view such as the velocity gradient tensor can be calculated using this view. Field statistics are easy to calculate from this Eulerian data as the individual flow fields can now be processed directly without need for binning but this also means that the benefits of the binning approach on Lagrangian data are not available. The spatial resolution is locked in by the resolution of a single snapshot and can not be increased simply by capturing more data as would be possible with a binning approach. We utilize the Eulerian flow fields for an event focused conditional averaging by using a quadrant analysis of the fluctuations as performed by (Schröder et al., 2011) for a turbulent boundary layer. Joint probability density functions for velocity fluctuation in the shear

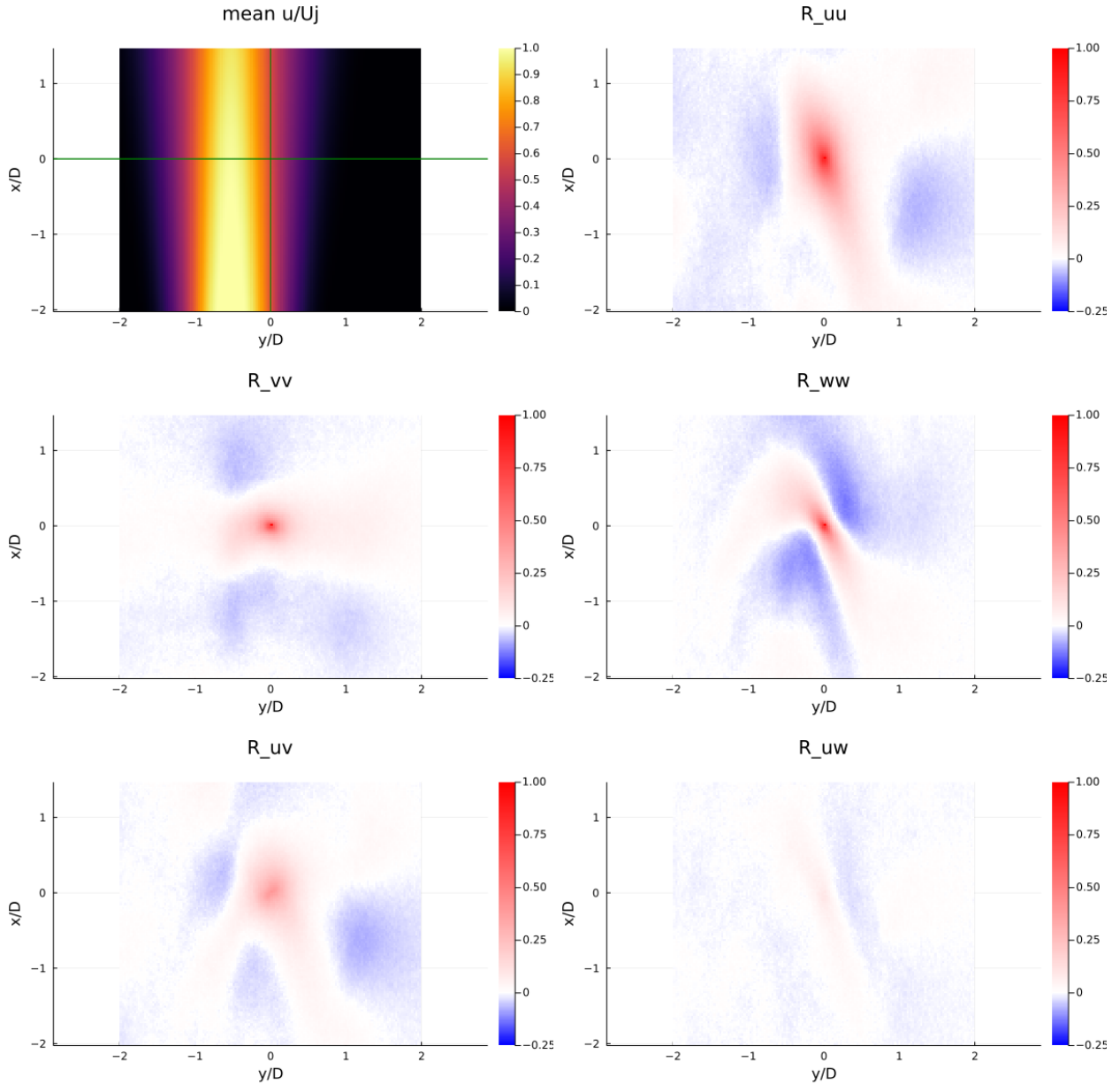

Figure 9. Two-point correlations for a point in the shear layer of the round jet on the lip-line approximately 4 nozzle diameters downstream of the nozzle. An asymmetric colormap is used to highlight regions with negative correlation value. The top left plot shows mean axial velocity field of the jet for orientation with reference point indicated by the cross.

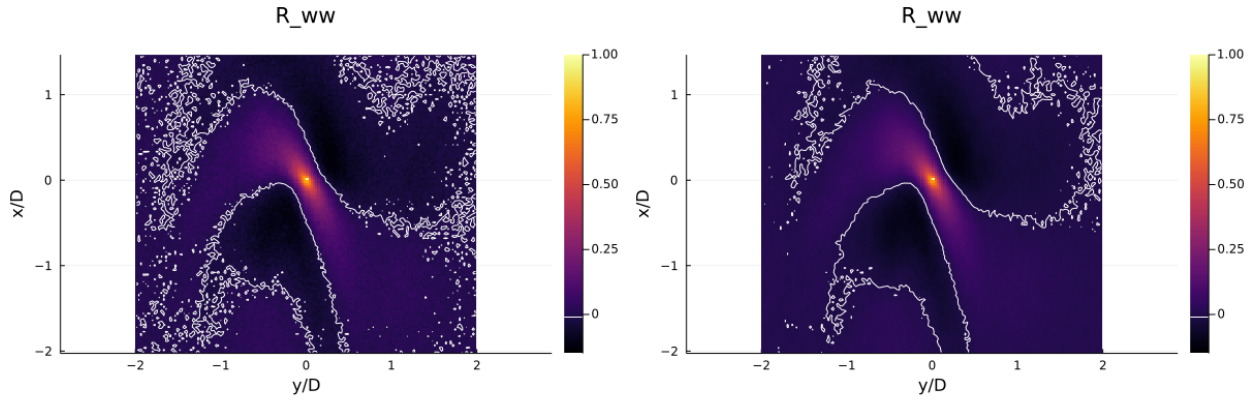

Figure 10. Two-point correlation with the same amount of approximately 50,000 snapshots using classic binning (left) and functional approach (right). The contour line for $R_{ww} = 0$ is shown in white highlighting the better convergence, especially in the further away regions.

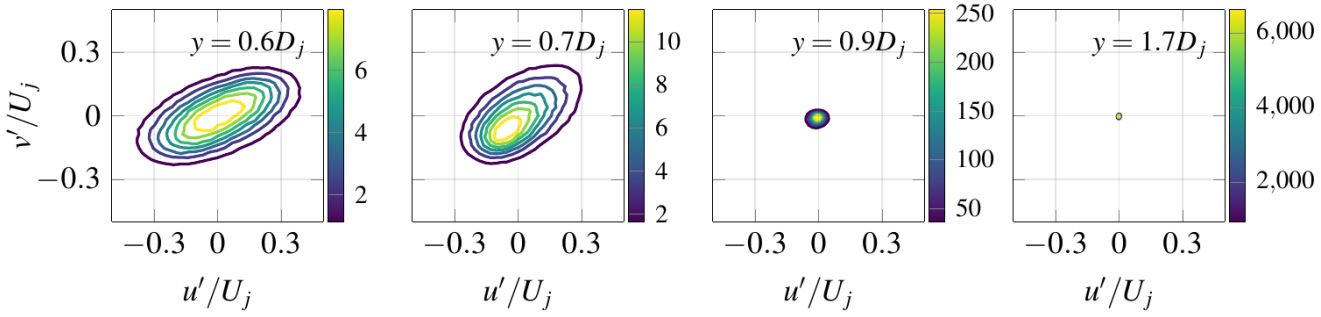

Figure 11. Joint probability density functions of u' and v' evaluated at various points along the line at approx. $3D_j$ downstream for the round nozzle. The statistics were calculated in a bin with size $2{\times}1{\times}1\,\mathrm{mm}^3$ around each point. Figure adapted from (Godbersen et al., 2019)

layer of the round jet are shown in figure 11. The alignment of the distribution in the quadrants, associated with "sweeps" and "ejections" is utilized to identify events for the conditional averaging. We now focus, as an example, on the top right quadrant where both fluctuation components are positive. For each Flowfit velocity field we search for voxels with fluctuation values that fall in that quadrant and extract them including a small neighborhood centered around each. These extracted events are then averaged over all events detected in all time steps. The averaging process reveals a mean structure of such detected events. Figure 12 shows the result of such an averaging process for the round jet for the quadrant $u' > 0, v' > 0$. Within the two ensemble averaged axial and radial velocity fluctuation we can witness such an averaged event. Since this analysis is performed on the FlowFit field the velocity gradient tensor is available so the vorticity can be studied as well. In the ensemble averaged field for the vorticity normal to the slice plane a strong footprint of such an event is apparent. For future investigations we desire to investigate such events in the shear layer together with the acoustic measurement. Unlike prior causality correlation approaches performed for this jet with the entire flow field, such a focus on correlating pressure fluctuations measured by far-field microphones to these individual nearly discrete events could provide a more direct link in terms of noise generation.

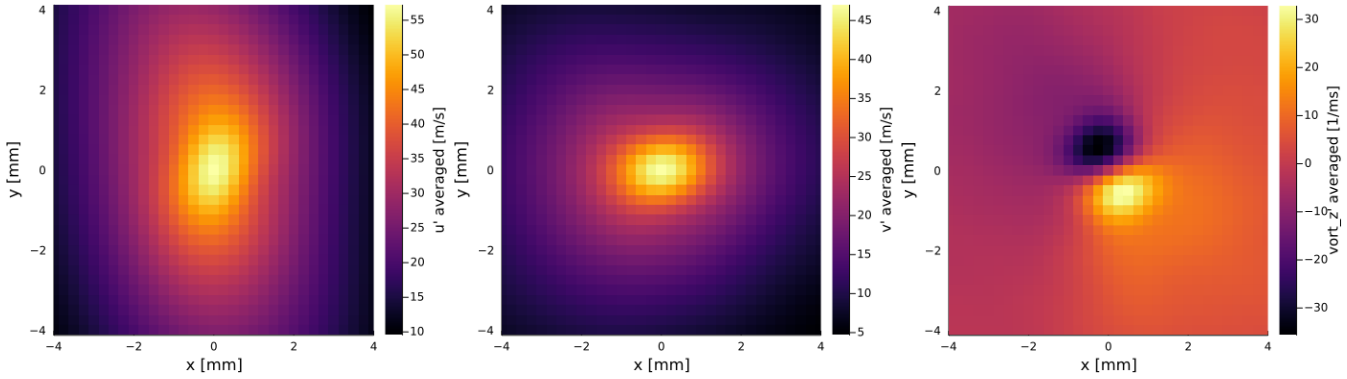

Figure 12. Conditionally averaged events extracted based on quadrant analysis for $u' > 0, v' > 0$: u′ (left), v′(middle), z-vorticity (right)

4. Outlook

As an outlook for the future we describe initial developments for a novel technique for the analysis of LPT data in line with the functional view on particle tracks already exploited here. This idea is based on the concept of control volumes as utilized for setting up balance equations for flow quantities where flux across the surfaces of the volume is counted. This is then used to set up balances for e.g. a kinetic energy balance by summing up the fluxes across the volume surfaces. We now introduce the LPT data to this concept, where we have measured tracks of fluid parcels. It is therefore possible to directly calculate where a fluid parcel crosses such a control volume boundary and which flow quantities it carries as shown in figure 13. As both velocity and acceleration are available for each fluid parcel, a wide variety of flux balances such as kinetic energy, force or impulse, could be created simply considering each parcel leaving and entering such a control volume. By averaging over a large number of available tracks, a balance of the fluxes over the surfaces can be established. The use of Lagrangian particle tracks enables small control volume sizes just as with functional binning. By utilizing a spatial binning analysis and a control volume analysis with the same bin and control volume sizes we can also perform balances of fluctuation quantities by subtracting mean values obtained from the binning. Combining these two approaches provides information about the statistics within the bin as well as fluxes over the surfaces. These quantities are of interest for example in tackling terms within the transport equation for turbulence kinetic energy.

$$k = \frac{1}{2}\left(\overline{(u')^2} + \overline{(v')^2} + \overline{(w')^2}\right) \tag{1}$$

$$\underbrace{\frac{\partial k}{\partial t}}_{\substack{\text{Local}\\ \text{derivative}}} + \underbrace{\overline{u}_j \frac{\partial k}{\partial x_j}}_{\text{Advection}} = \underbrace{-\frac{1}{\rho_o}\frac{\partial \overline{u_i' p'}}{\partial x_i}}_{\substack{\text{Pressure}\\ \text{diffusion}}} \underbrace{-\frac{1}{2}\frac{\partial \overline{u_j' u_j' u_i'}}{\partial x_i}}_{\substack{\text{Turbulent}\\ \text{transport}\\ \mathcal{T}}} + \underbrace{\nu \frac{\partial^2 k}{\partial x_j^2}}_{\substack{\text{Molecular}\\ \text{viscous}\\ \text{transport}}} \underbrace{-\overline{u_i' u_j'}\frac{\partial \overline{u_i}}{\partial x_j}}_{\substack{\text{Production}\\ \mathcal{P}}} \underbrace{-\nu \overline{\frac{\partial u_i'}{\partial x_j}\frac{\partial u_i'}{\partial x_j}}}_{\substack{\text{Dissipation}\\ \varepsilon_k}} \underbrace{-\frac{g}{\rho_o}\overline{\rho' u_i'}\delta_{i3}}_{\substack{\text{Buoyancy flux}\\ b}} \tag{2}$$

If we can directly calculate the convective transport of velocity fluctuation/ turbulence kinetic

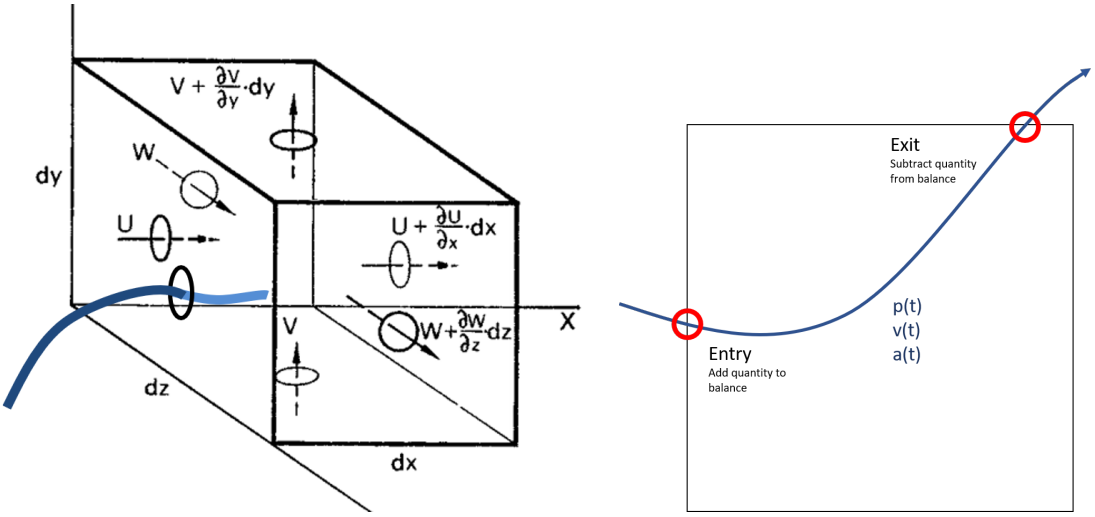

Figure 13. Left: Control volume for flux balance calculation with Lagrangian track piercing the surface. Figure adapted from (Bradshaw, 1971). Right: 2D sketch of a particle track passing trough a control volumes boundaries. The intersection with a boundary is determined by solving a quadratic equation for each intersection possibility of the different dimensions.

energy over the control volume boundaries as well utilize flow statistics for the control volume bin, such as Reynolds stresses or higher correlations, that would allow some terms on the right hand side of the transport equation for turbulent kinetic energy to be determined. Terms such as the production can be calculated from the bin average data alone as Reynolds stresses and mean velocities are readily available and gradients can be calculated across bins and similar considerations can be made for such terms as the turbulent transport and others. With the control volume approach where the measured Lagrangian tracks transport turbulence kinetic energy in and out of the control volume one would gain access to the left hand side of the transport equation. These quantities together might provide a pathway towards better estimation of the more illusive terms within that equation. Implementation of the control volume balance requires identifying the intersection of tracks with the volume boundaries. In our case, tracks are represented by polynomial of second degree so this can be achieved by solving a quadratic polynomial for each coordinate direction and interface for each track. Once an actual intersection point with a face of a control volume has been identified, the track can be simply evaluated at that position and the desired flow quantity can be added or subtracted from the balanced value based on the face normal. So far the balancing of flow quantities in and out of a volume is implemented but more work is needed for applying this idea and in order to present results.

Acknowledgements

Computer resources for this project have been provided by the Gauss Centre for Supercomputing/Leibniz Supercomputing Centre under grant: pr62zi.

References

Bradshaw, P. (1971). *An introduction to turbulence and its measurement*. Pergamon.

Gesemann, S., Huhn, F., Schanz, D., & Schröder, A. (2016). From noisy particle tracks to velocity and acceleration and pressure fields and using b-splines and penalties. In *18th international symposium on the application of laser and imaging techniques to fluid mechanics lisbon.*

Godbersen, P., Manovski, P., Novara, M., Schanz, D., Geisler, R., Mohan, N. K. D., & Schröder, A. (2019). Flow field analysis of subsonic jets at mach 0.5 and 0.84 using 3D multi pulse STB. In *Conference proceedings of the 13th international symposium on particle image velocimetry* (pp. 545–554).

Godbersen, P., & Schröder, A. (2020). Functional binning: improving convergence of eulerian statistics from lagrangian particle tracking. *Measurement Science and Technology*, *31*(9), 095304.

Godbersen, P., & Schröder, A. (2021). Enhanced functional binning for one-and two-point statistics using a posteriori uncertainty quantification of lpt data. In *14th international symposium on particle image velocimetry* (Vol. 1).

Maas, H. G., Gruen, A., & Papantoniou, D. (1993, jul). Particle tracking velocimetry in three-dimensional flows. *Experiments in Fluids*, *15*(2), 133–146. doi:

Manovski, P., Novara, M., Depuru Mohan, N. K., Geisler, R., Schanz, D., Agocs, J., … Schröder, A. (2021). 3d lagrangian particle tracking of a subsonic jet using multi-pulse shake-the-box. *Experimental Thermal and Fluid Science*, *123*, 110346. doi:

Miguel, E., & Henning, A. (2013). Analysis of simultaneous measurement of acoustic pressure in the far-field and density gradient in the near-field in a cold jet. In *19th aiaa/ceas aeroacoustics conference* (p. 2034).

Novara, M., Schanz, D., Reuther, N., Kähler, C. J., & Schröder, A. (2016, jul). Lagrangian 3D particle tracking in high-speed flows: Shake-The-Box for multi-pulse systems. *Experiments in Fluids*, *57*(8). doi:

Schanz, D., Gesemann, S., & Schröder, A. (2016, apr). Shake-The-Box: Lagrangian particle tracking at high particle image densities. *Experiments in Fluids*, *57*(5). doi:

Schröder, A., Geisler, R., Staack, K. é. a. a., Elsinga, G., Scarano, F., Wieneke, B., … Westerweel, J. (2011). Eulerian and lagrangian views of a turbulent boundary layer flow using time-resolved tomographic piv. *Experiments in fluids*, *50*(4), 1071–1091.

Sellappan, P., Alvi, F. S., & Cattafesta, L. N. (2020). Lagrangian and eulerian measurements in high-speed jets using multi-pulse shake-the-box and fine scale reconstruction (vic#). *Experiments in Fluids*, *61*(7), 1–17.